HHS Public Access

Author manuscript

Oncogene. Author manuscript; available in PMC 2013 March 06.

Published in final edited form as:

Oncogene. 2012 September 6; 31(36): 4034–4044. doi:10.1038/onc.2011.566.

Mcm2 deficiency results in short deletions allowing high resolution identification of genes contributing to lymphoblastic lymphoma

Michael E. Rusiniak, **Dimiter Kunnev**, **Amy Freeland**, **Gillian K. Cady**, and **Steven C. Pruitt***

Department of Molecular and Cellular Biology, Roswell Park Cancer Institute, Elm and Carlton Streets, Buffalo, NY 14263, USA

Abstract

Mini-chromosome maintenance (Mcm) proteins are part of the replication licensing complex that is loaded onto chromatin during the G1-phase of the cell cycle and required for initiation of DNA replication in the subsequent S-phase. Mcm proteins are typically loaded in excess of the number of locations that are utilized during S-phase. Nonetheless, partial depletion of Mcm proteins leads to cancers and stem cell deficiencies. Mcm2 deficient mice, on a 129Sv genetic background, display a high rate of thymic lymphoblastic lymphoma. Here array comparative genomic hybridization (aCGH) is utilized to characterize the genetic damage accruing in these tumors. The predominant events are deletions averaging less than 0.5 Mb, considerably shorter than observed in prior studies using alternative mouse lymphoma models or human tumors. Such deletions facilitate identification of specific genes and pathways responsible for the tumors. Mutations in many genes that have been implicated in human lymphomas are recapitulated in this mouse model. These features, and the fact that the mutation underlying the accelerated genetic damage does not target a specific gene or pathway a priori, are valuable features of this mouse model for identification of tumor suppressor genes. Genes affected in all tumors include *Pten*, *Tcfe2a*, *Mbd3* and *Setd1b*. *Notch1* and additional genes are affected in subsets of tumors. The high frequency of relatively short deletions is consistent with elevated recombination between nearby stalled replication forks in Mcm2 deficient mice.

Keywords

DNA replication; licensing factor; dormant origins; lymphoblastic lymphoma; Mcm2

Introduction

Minichromosome maintenance protein (Mcm) deficiency or hypomorphic function in mice has been shown to result in high rates of cancer where the specific cancer type shows a strong dependence on the genetic background on which the deficiency occurs (Shima et al.,

*Corresponding author: Telephone – 716-845-3589, steven.pruitt@roswellpark.org.

No conflict of interest is declared.

2007; Pruitt et al., 2007; Kunnev et al., 2010; Chuang et al., 2010). Mcm deficiency has been linked to increased rates of genetic damage in several studies. The Mcm4^{Chaos3} mutation was identified on the basis of a chromosomal instability phenotype (Shima et al., 2007). Further, abnormal karyotypes and elevated levels of chromosome breaks occur in cultured cells in which Mcm expression has been suppressed (Ge et al., 2007; Ibarra et al., 2008; Orr et al., 2010) and elevated rates of LOH are observed in clonal neural stem cells derived from Mcm2 deficient mice (Kunnev et al., 2010).

Mcm proteins are a family of replication licensing proteins where Mcm's 2–7 form a hexameric complex that is recruited to the chromatin early in the G1-phase of the cell cycle. The complex is thought to function, during the subsequent S-phase, as the replicative helicase. This function is important in both the initial unwinding of DNA at origins of replication and for fork extension (e.g. Blow and Dutta, 2005). However, in cells in culture reduced Mcm concentration does not affect the rate of fork elongation but does influence the ability of cells to initiate replication at dormant (lower efficiency) origins following treatment with agents that induce fork stalling (Ge et al., 2007; Ibarra et al., 2008; Kunnev et al., 2010). Hence, elevated levels of genetic damage in cells in culture and increased cancer rates in Mcm deficient mice may result from inefficient prereplicative complex assembly or origin usage.

In this study a strain of mice (Mcm2$^{IRES-CreERT2}$, referred to as Mcm2^{def} in this report) in which Mcm2 is expressed at approximately one third of wild type levels (Pruitt et al., 2007) is used to define the sites of genetic damage in the tumors that arise in these mice by aCGH.

Results

aCGH analysis of thymic tumors arising in Mcm2 deficient mice

Mcm2^{def} mice develop thymic tumors with 100% penetrance when carried on a 129/Sv genetic background (Pruitt et al., 2007; Kunnev et al., 2010). The disease is frequently disseminated affecting multiple lymph nodes, the spleen and other organs. That the tumors arising in these mice are from the T-cell lineage was confirmed by staining for CD3 (T-cell) and B220 (B-cell) markers (Supplemental Figure 1). The majority of cells present in these tumors and at disseminated sites (not shown) are CD3 positive and B220 negative consistent with T-lymphoblastic lymphoma.

Nimblegen 720K whole-genome tiling arrays were used to characterize copy number changes across the genome in 8 tumors arising in homozygous Mcm2^{def} mice on 129/Sv (6) or 129/Sv;C57Bl/6 F1 (2) genetic backgrounds. Additionally, DNA from paired non-tumorous tissue (tail) was examined for mice from which three of the tumors on the 129/Sv genetic background were derived. All 129/Sv derived samples were assessed relative to the same reference DNA from a wt 129/Sv littermate and 129/Sv;C57Bl/6 samples were similarly assessed relative to DNA from a single wt litter mate from an F1 cross of heterozygous Mcm2 deficient transgenic mice on the different strains. Analysis of non-tumorous tissue identified two short regions of copy number loss in a subset of mice (within the wdr5 and nlgn1 genes). The Mcm2 deficiency transgene is carried on the 129/Sv and other backgrounds as heterozygotes and it is unclear if the transgene contributes to

heterogeneity within the strains. Nonetheless the large majority of CNVs seen in tumors were not found in non-tumorous tissue suggesting that they were somatically derived. A summary of all haploid and diploid copy number variations (CNVs) for each tumor are shown mapped to individual chromosomes in Supplemental Figure 2. Higher resolution data for two regions, the Pten gene on chr 19 and the notch1 gene on chr2, are shown in Figure 1.

There are several general features of the CNVs occurring in these tumors that differ from those observed in prior studies in which CNVs were characterized from tumors arising in genetically engineered mice carrying other tumor promoting mutations (e.g. Maser et al., 2007; De Keersmaecker et al., 2010). First, the number of genetic changes resulting in deletions (avg. 20.6 per tumor) far exceeds those resulting in amplifications (avg. 2.2 per tumor); whereas in prior studies CNVs are typically distributed evenly between deletions and amplifications. Second, the intervals covered by the deletions found here are substantially smaller than those observed in prior studies in which the average size ranged between several and tens of Mb's. In contrast, the average deletion in thymic lymphomas arising on Mcm2 deficient mice is ~464 kb. Finally, there is a high degree of overlap between the CNVs occurring in different specific tumors. These features of the genomic changes occurring in tumors arising in Mcm2 deficient mice allow identification of genetic lesions contributing to tumorigenesis at high resolution using a minimal number of animals.

From the eight tumors analyzed, 21 minimal common deleted regions (MCDR) averaging 68.5 kb and 5 minimal common amplified regions (MCAR) averaging 0.40 Mb were identified (Figure 2). [MCRs were also identified in the TCR-α (Chr14), TCR-β (Chr6), and TCR-γ (Chr13) genes as is expected due to normal biological function and these MCRs are not included in the totals).] The size of the common regions is sufficiently small that in 12 of 21 MCDRs, and 4 of 5 MCARs, a single gene could be localized to the common intervals. Further, the pattern of deletions over 5 of the remaining MCDRs is consistent with the presence of two genes within the interval that contribute independently to selection for tumorigenic growth and, in these cases, 9 specific genes can be uniquely localized. Only 6 MCDRs of 21 contain more than a single candidate gene where one of these intervals includes only *Cdkn2a* and *Cdkn2b*. In total, 25 specific genes in unique-gene MCRs and 27 candidate genes distributed over 6 multi-gene MCRs were identified. These 52 genes were assessed for involvement in human cancers using the Catalogue of Somatic Mutations in Cancer (cosmic) and 70% of the MCRs, and 50% of the total genes, were shown to have previously identified mutations in human cancers. These observations provide insight into both the mechanism by which Mcm2 deficiency induces genetic damage and the genes and pathways contributing to T-lymphoblastic lymphomas.

Confirmation of deletions by sequencing fusion junctions

To confirm that chromosomal deletions identified by aCGH are present in tumors, oligonucleotide primers spanning predicted deleted regions from the notch1 and Pten loci were used to generate amplicons containing breakpoint junctions from tumor DNAs by PCR. In the case of notch1, amplicons containing junction fragments were obtained and sequenced for 3 tumors. The location of 5' and 3' junctions for the deletions identified in each of these tumors is shown on a map of the notch1 gene in Figure 3, panel A. Tumors

7302 and 7702 each carry deletions resulting in in-frame fusions between exons 2 and 28. The predicted proteins resulting from these fusions carry a truncated and likely non-functional EGF-like domain fused to a near complete notch1 intracellular domain (ICN1) and are likely to result in constitutively activate notch signaling. The deletion in tumor 8002 occurs between a location within exon 4 and 5' to exon 28 resulting in a prematurely truncated reading frame. Translation initiating at the normal start site would encode a polypeptide consisting of only EGF-like domains. However, prior studies have demonstrated the presence of a cryptic promoter within exon 29 (Jeannet et al. 2010) and transcripts initiating at this promoter are predicted to initiate translation at methionine 1796, which would again result in an activated notch1 intracellular domain. The locations at which notch1 deletions occur in tumors arising on Mcm2 deficient mice are not consistent with the illegitimate V(D)J recombination events (as indicated in Figure 3, panel A) that are frequently observed in other mouse models of T-ALL.

Junctions resulting from Pten deletions were also defined for several tumors (Figure 3, panel B). In each of these cases, the deletions are expected to result in loss of Pten function. Comparison of the sequences present at the 5' and 3' breakpoints of notch1 and Pten deletions is shown in Figure 4. There is no evidence for micro-homologies between the 5' and 3' breakpoints. In one Pten deletion a 61nt non-templated insertion is present. On average the sequences flanking the breakpoints are ~57% AT in composition and homo-polymeric A or T runs are found in several of the sequences.

Genes and pathways implicated in T-LL's arising on Mcm2 deficient mice

The most frequently occurring CNVs are deletions on Chr19 that overlap the *Pten* gene. All of the tumors assessed contain a diploid deletion overlapping *Pten* and the MCDR defined by these CNVs includes only this gene (Figure 1, panel A). Pten is a plasma-membrane lipid phosphatase that antagonizes the PI3K (phosphoinositide 3 kinase)-AKT pathway (reviewed in Buckler et al., 2008). Despite the bi-allelic loss of the *Pten* gene in all of the tumors assessed, subsets of tumors exhibit additional mutations in a large number of genes that either modulate PI3K activity or are PI3K targets. These include bi-allellic deletion of the PI3K inhibitors *Inppl1* and *Pitpnc1(Ship2)* and the amplification of the PI3K target *Vav1* (Figure 5).

A second frequent set of mutations affects *Tcfe2a* that encodes the E-box binding proteins E12 and E47. Seven of the eight tumor samples exhibit bi-allelic loss of *Tcfe2a* and the eighth (7802) shows loss of one allele. E2A activity is known to modulate the cell cycle during lymphoid cell maturation where *Cdkn1a* (p21cip1) is a key target (Yang et al., 2008). Two tumors, including 7802, exhibit bi-allelic loss of *Cdkna1* and this loss may complement the mono-allelic loss of E2A in this tumor (Figure 5).

Mbd3 is closely linked to *Tcfe2a* on Chr10 and many of the same deletion events that result in loss of *Mbd3* also affect *Tcfe2a*. Nonetheless, in the case of tumor 7802, which shows only mono-allelic loss of *Tcfe2a*, bi-allelic loss of *Mbd3* has occurred. This observation suggests that loss of *Mbd3* can, independently, provide a selective advantage in T-LLs. Consistent with this interpretation, both tumor 7002 and tumor 8102, in which bi-allelic loss of *Tcfe2a* and mono-allelic loss of *Mbd3* is observed, show loss of additional genes related

to Mbd3 function. Mbd3 is a component of the Mi2-NuRD complex which functions in chromatin remodeling through histone-deacetylase activity. Mi2-NuRD has been shown to play a role both in maintaining hematopoietic stem cell pools and in normal lineage progression (Ramírez and Hagman, 2009). In addition to Mbd proteins and histone deacetylases, the Mi2-NuRD complex is comprised of a number of additional proteins including Gatad2a (p66 alpha; Brackertz et al., 2002). In lymphocytes, the zinc finger DNA-binding factors Ikaros (Ikzf1), Aiolos (Ikzf3) and/or Helios (Ikzf2) are also associated with the complex and may function to impart DNA sequence specificity to Mi-2/NuRD complexes (Ramírez and Hagman, 2009). Tumor 7002 shows bi-allelic loss of *Gatad2a*, which is specific to this tumor (Figure 5). Similarly, tumor 8102 shows bi-allelic loss of *Ikzf1*, which again is specific to this tumor. Dnmt3a has also been reported to associate with the Mi-2/NuRD complex and tumor 8102 shows bi-allelic loss of this gene as well. Despite the bi-allelic loss of *Mbd3* function, *Dnmt3a* is also lost in tumor 7702 and *Ikzf3* is lost in tumor 7602, demonstrating redundancy in targeting of this pathway similar to the situation for PI3K signaling.

A third gene that undergoes bi-allelic loss in at least seven of the eight tumors analyzed is the histone H3-Lys^4 methyltransferase *Setd1b*. Mono-allelic loss of this gene is also found in the remaining tumor (7602). Additional related family members include Setd1a, MLL and the interacting protein Wdr5. CNVs in these genes are found in a subset of the tumors in which *Setd1b* is also lost. Setd1 complexes are localized to euchromatic regions of the genome, but different Setd1 family members are localized to non-overlapping domains suggesting that their functions are non-redundant. An additional cluster of mutations that may affect processes related to the Setd1 complex mutants occurs in components of the BAF and NURF complexes that link histone methylation to chromatin remodeling. Brpf3 function is compromised in each of the five tumors that fail to show an alteration in *Wdr5* (which as discussed above may be compromised in the germ line of a subset of the mice in this line). Additional chromatin remodeling complex components (Smard2, Myst1, Mllt1, and Bptf) are also compromised in smaller subsets of tumors (Figure 5).

Bi-allelic deletions in *Rnf40 (Bre1)* that are also likely to affect chromatin structure and gene activity are found in 5 of the 8 tumors (Figure 5). Rnf40 is recruited to active genes and is the E3 ligase for H2B ubiquitylation (Kim et al., 2009). H2B ubiquitylation has been shown to directly stimulate both hDOT1L-mediated H3K79 methylation and hSET1 complex-mediated H3K4 di- and tri-methylation and may play a role in maintaining an open chromatin configuration in active genes following RNA polymerase passage.

The notch signaling pathway is well established to contribute to T-cell lymphomas and activated forms of notch 1 are found in more than 50% of human tumors. CNVs are found in *notch 1* in four of the eight thymic lymphomas assayed here (Figure 3, Panel B, and Figure 5). As discussed above, in each of 3 cases confirmed by sequencing an internal deletion consistent with the generation of activating notch mutations has occurred. In three of the four remaining tumors which do not carry a CNV in *notch 1*, amplification of *cyclin G-associated kinase (Gak)* occurs (Figure 5). *Gak* is an auxilin related gene that has been shown to enhance notch signaling in zebrafish (Bai et al., 2010) and may play a role is elevating notch signaling in tumors in the present study. *Cdkn1a* is repressed by notch and

this repression has been shown to mediate much of the effect of notch on the cell cycle. Tumor 7802, in which both *notch* and *Gak* genes are unaffected, carries a bi-alleleic deletion of *Cdkn1a*.

Several additional recurrent CNVs that are not shown in Figure 5 have also been identified and are provided in Supplementary Figure 3. These include the gene encoding the centromere associated protein Cenp-o, on Chr12, the cGMP activated phosphodiesterase *Pde2a* on Chr7, *Wasf2* (*Wave2*) on Chr4 that mediates signals from tyrosine kinase receptors and small GTPases to the actin cytoskeleton, *septin 9*, which plays a role in filament assembly and potentially affects multiple cellular processes including cell division and chromosome segregation, and *reticulon 4 like receptor* which is known to function in the nervous system but is also expressed in the thymus. Two additional transcription factors, *Zfand3* on Chr17 and *Rfxdc2* (*Rfx7*) on Chr9, are also identified by recurrent bi-allelic deletions. Zfand3 is a zinc-finger protein containing a poly-ubiquitin binding domain and has been implicated in cellular differentiation of ES cells (Nishiyama et al., 2009). Rfxdc2 is a ubiquitously expressed winged-helix class transcription factor of unknown function (Aftab et al., 2008). Finally, recurrent diploid deletions occur in regions of Chr12 (108,379,999-108,459,999) and ChrX (132,813,333-132,946,667) and include locations where there are no known genes but at which predicted genes are located.

Comparison of CNVs in T-LLs arising in Mcm2 deficient mice with CNVs in human T-ALLs

To examine the relationship between the CNVs occurring in T-LLs of Mcm2 deficient mice with those found in prior studies of human T-ALLs, the locations of MCRs for recurrent CNVs from three prior studies (Kuiper et al., 2007; Mullighan et al., 2007; Remke et al., 2009) in which CNVs were examined for either 7, 50 or 73 human (largely childhood) T-ALLs were compared to the locations of genes identified by MCRs of recurrent CNVs in mouse tumors (Table I). As in the mouse tumors studied here, deletions affecting the locus encoding Cdkn2a and Cdkn2b genes and the Pten gene are identified in human T-ALLs. Comparison of the mouse and human data sets has also identified locations on human Chr19 p13.3 and Chr19p13.2 that contain amplifications near to the location of genes that are also affected in mouse tumors. This region of the human genome is syntenic with four chromosomal locations in the mouse from Chr10, Chr17, Chr9 and Chr8 two of which show CNV in the present study (Supplementary Figure 4). The syntenic region of mouse Chr17 includes the region between Mtl1 and Vav1 and shows recurrent amplification in the mouse tumors. The syntenic region of mouse Chr10 spans the region from Mbd3-Sirt6 and includes the Tcf-e2a gene. As discussed above, Mbd3 and Tcf-e2a are sites of highly recurrent deletions in the mouse tumors. Whether amplification of the Mbd3 or Tcf-e2a genes in human cells compromises their functions is at present unclear. Additionally, the region of human Chr19 that is syntenic to mouse Chr9 contains a series of MBD3 related genes, MBD3L2–5. Two related family members, Mbd3l1 and Mbd3l2, are found on Chr9 in the mouse but are not affected by CNVs in mouse tumors. Whether the amplifications observed in humans affects the MBD3L2–5 genes to compromise the same pathway as Mbd3 deletion in the mouse is at present unclear but may be important to investigate in additional studies. Further, these observations illustrate the potential effects that the different organizations of

the mouse and human genomes may have on the types of genomic alterations that are necessary to result in tumorigenesis even though similar pathways may be affected.

One feature that is apparent from data on human tumors is that, with the exception of the CNVs affecting the CDKN2A and CDKN2B genes, even recurrent CNVs in human tumors affect only a small subset, less than 10%, of tumors (Mullighan et al., 2007; Kuiper et al., 2007; Remke et al., 2009). Since only 8 mouse tumors were assessed in the present study, diploid deletion in even one tumor represents a rate of occurrence of 12.5%, higher than most of the recurrent CNVs identified in human T-ALLs. If these cases are also considered, genes affected in mouse tumors that are also present at sites of CNV in the human data sets include Ikzf1(human chr 7p12.2) and Mll1 (human chr 11q23.3).

Non-recurrent haploid deletions are shorter than average

A subset of CNVs found in the mouse tumors described here was non-recurrent and exhibited an average $\log_2$ ratio consistent with deletion of one chromosomal copy (<0.4). A few of these events occurred in genes that could be related to pathways implicated in tumorigenesis (e.g. Nedd4) and these were removed from further consideration. A total of 13 non-recurrent, haploid, deletion events that occurred in regions that either contain no known gene or contained a gene(s) unlikely to be related to tumorigenesis were identified and are considered to represent passenger mutations. Since passenger mutations occur in cells prior to selection for genes driving tumorigenesis, this subset of CNVs may most closely reflect the effects of Mcm2 deficiency on genome stability. A comparison of the size distribution of the putative passenger mutations (panel B) with those of all deletions or amplifications (panel A) is shown in Figure 6. This comparison shows that the subset of deletions identified as passenger mutations is even shorter than the average of all deletions (average size 145 kbp compared to 464 kbp).

Discussion

Several studies have demonstrated that reduced Mcm concentrations result in elevated genetic damage (Shima et al., 2007; Pruitt et al., 2007; Ge et al., 2007; Ibarra et al. 2008; Orr et al., 2010; Kunnev et al., 2010). The present study extends this observation by showing that the genetic damage accruing in tumors arising in Mcm2 deficient mice exhibits an unusual pattern of chromosomal damage in which the majority of chromosomal aberrations are deletions and in which the average size of the deletions is substantially shorter than those observed in other mouse cancer models including those that develop a high proportion of T-LLs (e.g. Maser et al., 2007).

One mechanism that could account for both the increased genomic instability and the accumulation of shorter deletion intervals in $Mcm2^{def}$ mice is if deletions are frequently a consequence of recombination between two, nearby, stalled replication forks. Specifically, under conditions of Mcm deficiency both the frequency of initiation at primary origins is expected to be reduced, increasing the likelihood of replication fork stalling, and the ability to overcome double stalled replication forks by reinitiation at an otherwise dormant origin is compromised, potentially resulting in fork collapse (Blow et al., 2011). Replication of different regions of the genome is segmented during S-phase such that active replication

origins are clustered and replicated together within replication factories that consist of between 4 and 20 replication forks (i.e. 2 – 10 origins where the average distance between origins is on the order of 50–100 kb). Dormant origin function is tightly linked to this organization through the DNA damage checkpoint kinases ATR and Chk1 (Ge and Blow, 2010; Blow et al., 2011). ATR and Chk1 inhibit the activation of new replication factories but allow dormant origins to fire within already active factories. One consequence of this organization is to focus dormant origin firing to active factories where rescue of stalled replication forks is required. Additionally, partitioning replication into relatively short domains that are physically and temporally discrete minimizes the possibility of interaction between two locations at which replication fork stalling has occurred, reducing the likelihood of recombination. It has been observed that there is a critical minimum threshold of between ~35 and 50% reduction in Mcm concentration at which phenotypic effects including cancer incidence are greatly accelerated (Chuang et al., 2010). The sizes of the deletions observed in tumors of Mcm2 deficient mice, where Mcm2 is expressed at a level just below this threshold, are consistent with recombination events within single replication factories and support the possibility that the threshold at which phenotypic effects of Mcm reduction are observed is a consequence of breaching this physical separation (Figure 7).

Analysis of the sequences present at deletion junctions in the notch 1 gene demonstrated that, unlike several other mouse transgenic lines that exhibit T-LL tumors, activating mutations do not result from illegitimate V(D)J recombination. Rather, the notch1 3’ deletion junctions fall within an approximately 200 nt long region of the notch1 gene between exons 27 and 28 that is AT rich and contains homo-polymeric runs of T and A and other short repeating sequences. Sequences present at breakpoints for three deletions in the Pten gene have similar properties. In addition, a short non-templated insertion is present at one junction. These properties are similar to those observed for sequences present at interstitial deletions in human tumors (Abeysinghe et al., 2003).

The remarkably short deletion intervals occurring in T-LLs arising on Mcm2 deficient mice provide a high level of resolution in defining specific genes that contribute to this disease. The genes and pathways identified as contributing to T-LLs in Mcm2 deficient mice share several similarities to those known to contribute to T-cell lymphomas in humans. Activating mutations in *notch1* have been found in more than half of human T-cell lymphomas (Weng et al., 2004) similar to the tumors arising in $Mcm2^{def}$ mice. Direct *Pten* mutations occur in more than 20% of human T-cell lymphomas, whereas hyper-activation of PI3K signaling occurs in more than 85% of cases (Palomero et al., 2007) and CNVs in genes affecting the PI3K signaling pathway are frequently observed in human T-ALLs (Remke et al., 2009). Finally, deletions affecting the locus encoding Cdkn2a and Cdkn2b genes are the most highly recurrent CNVs in human T-ALLs (Williams and Sherr, 2008) and 25% of the Mcm2 deficient mouse tumors are similarly affected.

However, many of the recurrent mutations found in Mcm2 deficient thymic tumors have not been associated with human T-ALLs. Nonetheless, mutations in a number of these genes have been found in other human hematological, and non-hematological, cancers. These include *Tcfe2a* (LeBrun, 2003), *Mll1* (Hess, 2004), *Mllt1* (Meyer et al., 2009), *Mllt10* (Meyer et al., 2009), *Ikzf1* (Collins-Underwood and Mullighan, 2010), *Ikzf3* (Rebollo and

Schmitt, 2003), *Bcl11b* (De Keersmaecker et al., 2010), *Bcl7a* (Zani et al., 1996), *Sept9* (Santos et al., 2010), *Vav1* (Katzav, 2009), DNMT3a (Ley et al., 2010) and *Asxl1* (Tefferi, 2010). The frequent mutation of known tumor suppressor genes in the tumors arising on Mcm2 deficient mice suggest that this data set is likely to contain additional novel tumor suppressor genes. The highly recurrent deletions in *Setd1b, Mbd3, Rnf40, and Brpf3*, all of which function in aspects of chromatin remodeling, implicate these genes in particular.

The strong tumorigenic effect of reduced Mcm concentrations in mice raises the issue of whether insufficient Mcm activity contributes to human lymphomas or human cancers generally. There is evidence from aCGH for the preferential loss of Mcm proteins 2, 6 and 7 (Supplemental Table II) in a modest subset of human tumors of various types whereas Mcm3 is preferentially amplified. The observation that Mcm3 copy number is increased is consistent with previous studies suggesting that this protein has a negative role in origin licensing. In vivo, reduced Mcm3 levels have been shown to partially rescue the cancer phenotype of mice carrying the Mcm4 mutant allele Chaos3 (Chuang et al., 2010). Finally, CNVs in a subset of human T-ALLs have been observed on human Chr 7q22.1 near the location of the Mcm7 gene (Remke et al., 2009).

Ineffective origin licensing may contribute to genome instability even in the absence of direct Mcm mutation or copy number alteration. The levels of Mcm proteins present in quiescent human T-lymphocytes are substantially lower than in cycling cells (Orr et al., 2010). Further, it has been shown that human T-lymphocytes exiting from quiescence are particularly sensitive to siRNA mediated reduction in Mcm concentration and rapidly acquire genetic damage (Orr et al., 2010). The present studies support that this process is accelerated in the Mcm2 deficient mouse model.

Materials and Methods

Mice

The mice used in this study are the transgenic line $Mcm2^{IRES\text{-}CreERT2}$ carried on a 129/Sv genetic background (Pruitt et al. 2007) and a congenic line in which the $Mcm2^{IRES\text{-}CreERT2}$ transgene was crossed into a C57Bl/6 genetic background through 6 generations. In each case the transgene is carried in heterozygotes. Thymic tumors arising on $Mcm2^{IRES\text{-}CreERT2}$ homozygous mice on the 129/Sv genetic background (6) or from the F1 generation of a cross between the 129 and C57Bl/6 congenic lines at between 2 and 4 months of age were resected and DNA was isolated for aCGH analysis using a Roche DNA Isolation Kit (11 814 770 001) as described by the manufacturer.

Array CGH

aCGH was performed on 720k Roche NimbleGen oligonucleotide arrays using DNAs isolated from the tumors described above and control DNAs derived from tails of mice of the same genetic backgrounds and from the same colonies as mice from which tumors were derived. Tumors 7002, 7302, 7402, 7602, 7902 and 8102 were derived from mice on a 129/Sv genetic background and tumors 7802 and 8002 were derived from F1 129/

Sv;C57Bl/6 mice. Data were analyzed using NimbleScan v2.6 and Signal Map 1.9.0.05 software.

Sequencing tumor deletion junctions

Amplicons bridging tumor deletion junctions as predicted by analysis of aCGH data were generated by PCR using Crimson LongAmp Taq DNA Polymerase (New England BioLabs) according to manufacturer's instructions, excised from 0.8% agarose gels, purified using the GeneJET Gel Extraction Kit (Fermentas) and sequenced.

Supplementary Material

Refer to Web version on PubMed Central for supplementary material.

Acknowledgments

This work was supported by grants from the NIH-NCI, the Ellison Medical Foundation, and NYSTEM to SCP. Cost of animal maintenance and flow cytometry was supported in part by an NCI-CCS grant to RPCI.

References

Abeysinghe SS, Chuzhanova N, Krawczak M, Ball EV, Cooper DN. Translocation and gross deletion breakpoints in human inherited disease and cancer I: Nucleotide composition and recombination-associated motifs. Human Mutation. 2003; 22:229. [PubMed: 12938088]

Aftab S, Semenec L, Chu JS, Chen N. Identification and characterization of novel human tissue-specific RFX transcription factors. BMC Evol Biol. 2008; 8:226. [PubMed: 18673564]

Bai T, Seebald JL, Kim KE, Ding HM, Szeto DP, Chang HC. Disruption of zebrafish cyclin G-associated kinase (GAK) function impairs the expression of Notch-dependent genes during neurogenesis and causes defects in neuronal development. BMC Dev Biol. 2010; 10:7. [PubMed: 20082716]

Blow JJ, Dutta A. Preventing re-replication of chromosomal DNA. Nat Rev. 2005; 6:476–486.

Blow JJ, Ge XQ, Jackson DA. How dormant origins promote complete genome replication. Trends Biochem Sci. 2011 [Epub ahead of print].

Brackertz M, Boeke J, Zhang R, Renkawitz R. Two highly related p66 proteins comprise a new family of potent transcriptional repressors interacting with MBD2 and MBD3. J Biol Chem. 2002; 277:40958–40966. [PubMed: 12183469]

Buckler JL, Liu X, Turka LA. Regulation of T-cell responses by PTEN. Immunol Rev. 2008; 224:239–248. [PubMed: 18759931]

Chuang CH, Wallace MD, Abratte C, Southard T, Schimenti JC. Incremental genetic perturbations to MCM2-7 expression and subcellular distribution reveal exquisite sensitivity of mice to DNA replication stress. PLoS Genet. 2010; 6:e1001110. [PubMed: 20838603]

Collins-Underwood JR, Mullighan CG. Genomic profiling of high-risk acute lymphoblastic leukemia. Leukemia. 2010; 24:1676–1685. [PubMed: 20739952]

De Keersmaecker K, Real PJ, Gatta GD, Palomero T, Sulis ML, Tosello V, et al. The TLX1 oncogene drives aneuploidy in T cell transformation. Nat Med. 2010; 16:1321–1327. [PubMed: 20972433]

Ge XQ, Jackson DA, Blow J. Dormant origins licensed by excess Mcm2-7 are required for human cells to survive replicative stress. Genes Dev. 2007; 21:3331–3341. [PubMed: 18079179]

Ge XQ, Blow JJ. Chk1 inhibits replication factory activation but allows dormant origin firing in existing factories. J Cell Biol. 2010; 191(7):1285–1297. [PubMed: 21173116]

Hess JL. Mechanisms of transformation by MLL. Crit Rev Eukaryot Gene Exp. 2004; 14:235–254.

Ibarra A, Schwob E, Méndez J. Excess MCM proteins protect human cells from replicative stress by licensing backup origins of replication. Proc Natl Acad Sci USA. 2008; 105:8956–8961. [PubMed: 18579778]

Jeannet R, Mastio J, Macias-Garcia A, Oravecz A, Ashworth T, Geimer Le Lay AS, Jost B, Le Gras S, Ghysdael J, Gridley T, Honjo T, Radtke F, Aster JC, Chan S, Kastner P. Oncogenic activation of the Notch1 gene by deletion of its promoter in Ikaros-deficient T-ALL. Blood. 2010; 116:5443–5454. [PubMed: 20829372]

Katzav S. Vav1: a hematopoietic signal transduction molecule involved in human malignancies. Int J Biochem Cell Biol. 2009; 41:1245–1248. [PubMed: 19100858]

Kim J, Guermah M, McGinty RK, Lee JS, Tang Z, Milne TA, et al. RAD6-Mediated transcription-coupled H2B ubiquitylation directly stimulates H3K4 methylation in human cells. Cell. 2009; 137:459–471. [PubMed: 19410543]

Kuiper RP, Schoenmakers EF, van Reijmersdal SV, Hehir-Kwa JY, van Kessel AG, van Leeuwen FN, Hoogerbrugge PM. High-resolution genomic profiling of childhood ALL reveals novel recurrent genetic lesions affecting pathways involved in lymphocyte differentiation and cell cycle progression. Leukemia. 2007; 21(6):1258–1266. [PubMed: 17443227]

Kunnev D, Rusiniak ME, Kudla A, Freeland A, Cady GK, Pruitt SC. DNA damage response and tumorigenesis in Mcm2-deficient mice. Oncogene. 2010; 29:3630–3638. [PubMed: 20440269]

LeBrun DP. E2A basic helix-loop-helix transcription factors in human leukemia. Front Biosci. 2003; 8:s206–s222. [PubMed: 12700034]

Ley TJ, Ding L, Walter MJ, McLellan MD, Lamprecht T, Larson DE, Kandoth C, Payton JE, Baty J, Welch J, Harris CC, Lichti CF, Townsend RR, Fulton RS, Dooling DJ, Koboldt DC, Schmidt H, Zhang Q, Osborne JR, Lin L, O'Laughlin M, McMichael JF, Delehaunty KD, McGrath SD, Fulton LA, Magrini VJ, Vickery TL, Hundal J, Cook LL, Conyers JJ, Swift GW, Reed JP, Alldredge PA, Wylie T, Walker J, Kalicki J, Watson MA, Heath S, Shannon WD, Varghese N, Nagarajan R, Westervelt P, Tomasson MH, Link DC, Graubert TA, DiPersio JF, Mardis ER, Wilson RK. DNMT3A mutations in acute myeloid leukemia. N Engl J Med. 2010 Dec 16; 363(25):2424–2433. [PubMed: 21067377]

Maser RS, Choudhury B, Campbell PJ, Feng B, Wong KK, Protopopov A, et al. Chromosomally unstable mouse tumours have genomic alterations similar to diverse human cancers. Nature. 2007; 447:966–971. [PubMed: 17515920]

Meyer C, Kowarz E, Hofmann J, Renneville A, Zuna J, Trka J, et al. New insights to the MLL recombinome of acute leukemias. Leukemia. 2009; 23:1490–1499. [PubMed: 19262598]

Mullighan CG, Goorha S, Radtke I, Miller CB, Coustan-Smith E, Dalton JD, Girtman K, Mathew S, Ma J, Pounds SB, Su X, Pui CH, Relling MV, Evans WE, Shurtleff SA, Downing JR. Genome-wide analysis of genetic alterations in acute lymphoblastic leukaemia. Nature. 2007; 446(7137): 758–764. [PubMed: 17344859]

Nishiyama A, Xin L, Sharov AA, Thomas M, Mowrer G, Meyers E, et al. Uncovering early response of gene regulatory networks in ESCs by systematic induction of transcription factors. Cell Stem Cell. 2009; 5:420–433. [PubMed: 19796622]

Orr SJ, Gaymes T, Ladon D, Chronis C, Czepulkowski B, Wang R. Reducing MCM levels in human primary T cells during the G(0)-->G(1) transition causes genomic instability during the first cell cycle. Oncogene. 2010; 29:3803–3814. [PubMed: 20440261]

Palomero T, Sulis ML, Cortina M, Real PJ, Barnes K, Ciofani M, et al. Mutational loss of PTEN induces resistance to NOTCH1 inhibition in T-cell leukemia. Nat Med. 2007; 13:1203–1210. [PubMed: 17873882]

Pruitt SC, Bailey KJ, Freeland A. Reduced Mcm2 expression results in severe stem/progenitor cell deficiency and cancer. Stem Cells. 2007; 25:3121–3132. [PubMed: 17717065]

Ramírez J, Hagman J. The Mi-2/NuRD complex: a critical epigenetic regulator of hematopoietic development, differentiation and cancer. Epigenetics. 2009; 4:532–536. [PubMed: 19923891]

Rebollo A, Schmitt C. Ikaros, Aiolos and Helios: transcription regulators and lymphoid malignancies. Immunol Cell Biol. 2003; 81:171–175. [PubMed: 12752680]

Remke M, Pfister S, Kox C, Toedt G, Becker N, Benner A, Werft W, Breit S, Liu S, Engel F, Wittmann A, Zimmermann M, Stanulla M, Schrappe M, Ludwig WD, Bartram CR, Radlwimmer B, Muckenthaler MU, Lichter P, Kulozik AE. High-resolution genomic profiling of childhood T-ALL reveals frequent copy-number alterations affecting the TGF-beta and PI3K-AKT pathways

and deletions at 6q15-16.1 as a genomic marker for unfavorable early treatment response. Blood. 2009; 114(5):1053–1062. [PubMed: 19406988]

Santos J, Cerveira N, Correia C, Lisboa S, Pinheiro M, Torres L, et al. Coexistence of alternative MLL-SEPT9 fusion transcripts in an acute myeloid leukemia with t(11;17)(q23;q25). Cancer Genet Cytogenet. 2010; 197:60–64. [PubMed: 20113838]

Shima N, Alcaraz A, Liachko I, Buske TR, Andrews CA, Munroe RJ, et al. A viable allele of Mcm4 causes chromosome instability and mammary adenocarcinomas in mice. Nat Genet. 2007; 39:93–98. [PubMed: 17143284]

Tefferi A. Novel mutations and their functional and clinical relevance in myeloproliferative neoplasms: JAK2, MPL, TET2, ASXL1, CBL, IDH and IKZF1. Leukemia. 2010; 24:1128–1138. [PubMed: 20428194]

Weng AP, Ferrando AA, Lee W, Morris JP 4th, Silverman LB, Sanchez-Irizarry C, et al. Activating mutations of NOTCH1 in human T cell acute lymphoblastic leukemia. Science. 2004; 306:269–271. [PubMed: 15472075]

Williams RT, Sherr CJ. The INK4-ARF (CDKN2A/B) locus in hematopoiesis and BCR-ABL-induced leukemias. Cold Spring Harb Symp Quant Biol. 2008; 73:461–467. [PubMed: 19028987]

Yang Q, Kardava L, St Leger A, Martincic K, Varnum-Finney B, Bernstein ID, et al. E47 controls the developmental integrity and cell cycle quiescence of multipotential hematopoietic progenitors. J Immunol. 2008; 181:5885–5894. [PubMed: 18941177]

Zani VJ, Asou N, Jadayel D, Heward JM, Shipley J, Nacheva E, et al. Molecular cloning of complex chromosomal translocation t(8;14;12)(q24.1;q32.3;q24.1) in a Burkitt lymphoma cell line defines a new gene (BCL7A) with homology to caldesmon. Blood. 1996; 87:3124–3134. [PubMed: 8605326]

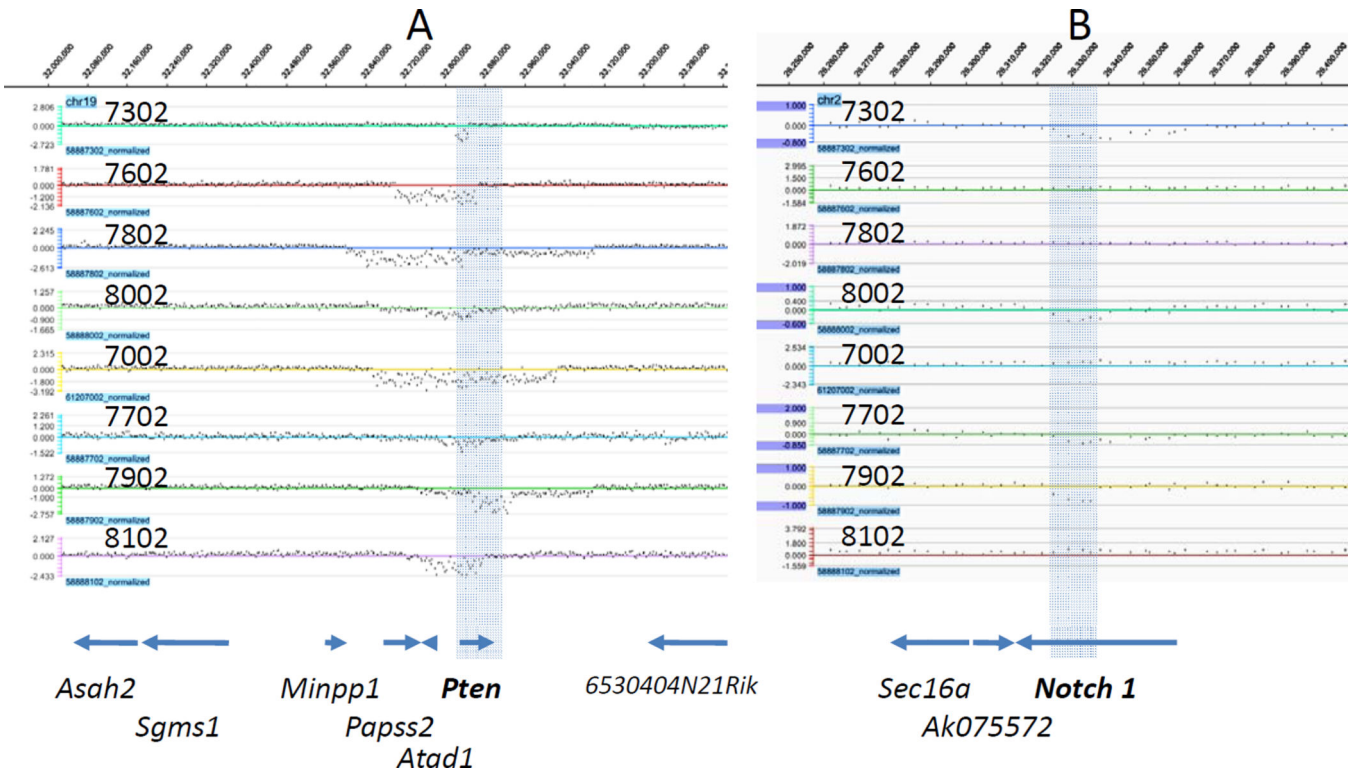

Figure 1.

aCGH for *Pten* and *notch 1* containing regions of Chr19 and Chr2. Array CGH signal tracks (log_2 ratios) for each of eight tumors as indicated by the tumor number are shown for the *Pten* region of Chr19 (Panel A) and the *notch1* region of Chr2 (Panel B). In each case the positions of genes as defined by the UCSC genome browser gene track from the mm9 sequence build is aligned below the aCGH tracks. The shaded region in A denotes the location of *Pten* across all tracks and the shaded region in B denotes the location of exons 5–22 of *notch1* across all tracks.

Deletions															
CNV No.	Frequency	Chromosome	Start	End	Size	Genes in Interval		7302	7602	7802	8002	7002	7702	7902	8102
1	8	chr19	32819999	32859999	40000	Pten	Simple	x	x	x	x	x	x	x	x
2	7	chr5	123578388	123593632	15244	Setd1b	Simple	x	h	x	x	x	x	x	x
3	7	chr10	79899999	79939999	40000	Tcfe2a	Complex	x	x	h	x	x	x	x	x
	7	chr10	79858188	79858188	0	Mbd3		x	x	x	x	h	x	x	h
4	5	chr7	134709080	134825954	116874	Phkg2; Gm166; Rnf40	Simple	x		x	x		x	x	
5	4	chr2	26324605	26337808	13203	notch 1	Simple	x			x		x	x	
6 *	4	chr3	25415559	25456523	40964	Nlgn1	Simple	x	x					x	x
7	4	chr12	4219999	4219999	0	Cenpo	Complex					x	x	x	x
	4	chr12	3859999	3899999	40000	Dnmt3a							x		x
8	4	chr17	28829446	29219999	390553	Mapk14; Mapk13; Brpf3; Pnpla1; 4930539E08Rik; Pxt1; Kctd20; Stk38; Sfrs3; AK144811	Simple			x		x	x		x
9	4	chr17	30287365	30181394	-105971	Zfand3	Complex	x			x	x	x		
	4	chr17	30474260	30579999	105739	Btbd9						x	x		
10		chrX	132813333	132946667	133334	predicted gene	Simple	x	x					x	x
11*	3	chr2	27349578	27363138	13560	Wdr5	Simple	x	x					x	
12	3	chr4	132699999	132699999	0	Wasf2	Complex		x					x	
	3	chr4	133104857	133110567	5710	shp						x		x	x
13	3	chr7	108660000	108579999	-80001	Pde2a	Simple					x		x	x
14	3	chr9	72339999	72419999	80000	Rfxdc2	Simple			x	x			x	
15	3	chr11	106540000	106579999	39999	Pecam1	Complex			x					x
	3	chr11	106780000	106939999	159999	Smurf2; Kpna2; Bptf						x			x
16	3	chr12	108379999	108459999	80000	XM_001474777	Simple				x			x	x
	3	chr12	109179999	109219999	40000	Bcl11b	Simple					x	x	x	
17	2	chr4	88899999	89059999	160000	Cdkn2a; Cdkn2b	Simple					x			x
18	2	chr11	75019999	75099999	80000	Rtn4rl1	Simple	x			x			x	
19	2	chr11	97779999	97859999	80000	Plxdc1	Simple		x					x	
20	2	chr11	98179999	98259999	80000	Neurod2; Ppp1r1b; Stard3; titin-cap; Pnmt; Perld1	Simple		x			x			
21	2	chr11	117179999	117456591	276592	Septin-9	Simple				x			x	
				Average Size	68362.92593		Total del	9	8	7	9	12	9	16	11
Amplifications															
CNV No.	Frequency	Chromosome	Start	End	Size	Genes in Interval		7302	7602	7802	8002	7002	7702	7902	8102
1	3	chr2	153167572	153176820	9248	Asxl1			x				x		x
2	3	chr5	108729594	109144476	414882	Gak			x			x			x
3	3	chr17	55952968	57447177	1494209	Mllt1; Chaf1a; Uhrf1; Dennd1c; vav 1			x			x			x
4	3	chrX	166346473	166406744	60271	Mid1							x	x	x
5	2	chr2	17972355	17988715	16360	Mllt10			x	x					
				Average Size	398994		Total amp	0	4	1	0	2	2	1	4
							Total CNV	9	12	8	9	14	11	17	15

Figure 2.

Chart of minimal common region intervals and candidate genes. The minimum common intervals of CNVs determined by aCGH are shown where the tumors exhibiting the CNVs are marked. CNV within MCRs 6 and 11 (marked with asterisks) were also found in a paired non-tumorous tissue from the same animals and may result from genetic heterogeneity within the strain.

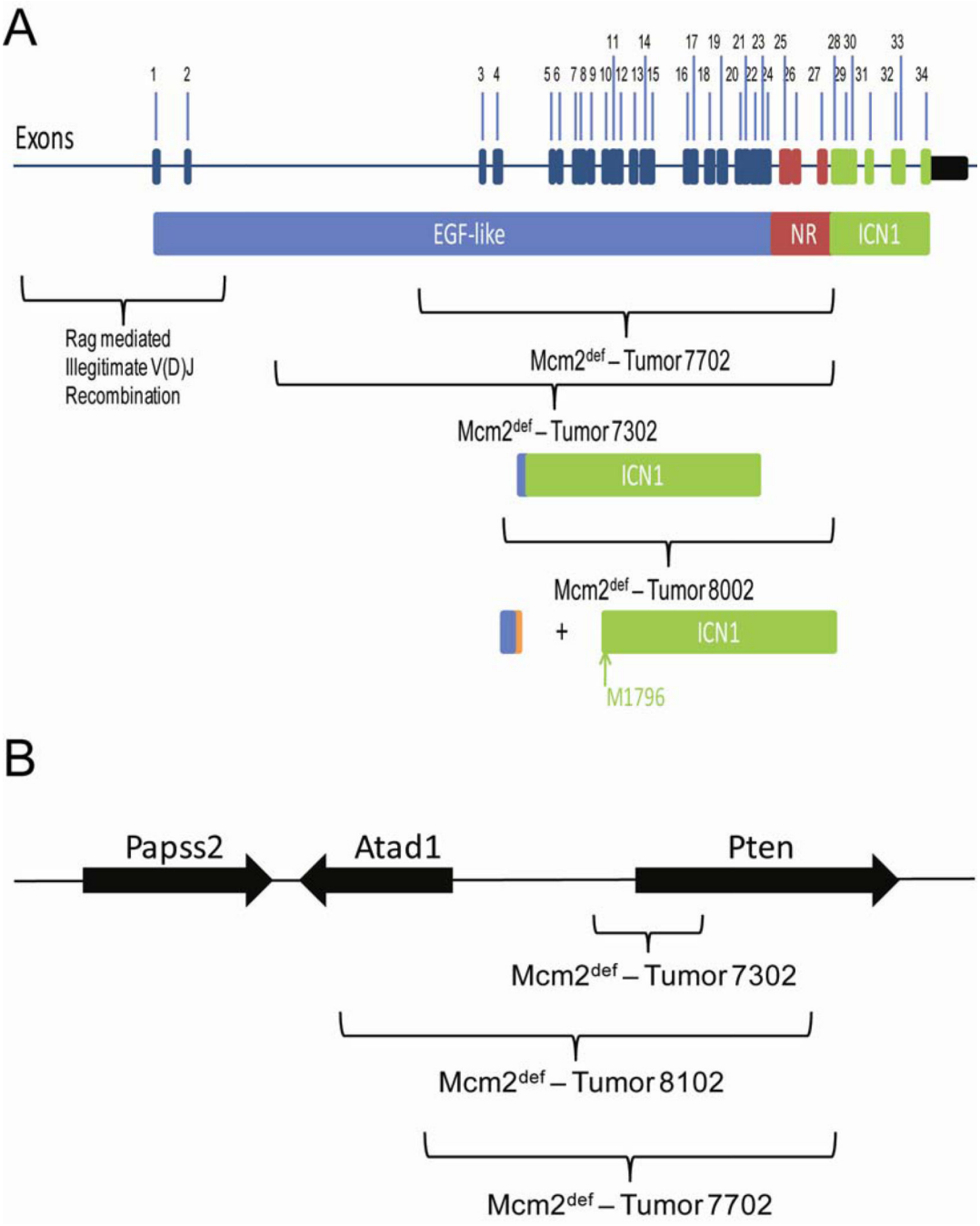

Figure 3.

Locations of deletion breakpoints at notch1 and Pten loci defined by sequencing breakpoint junctions. Panel A shows the notch1 locus where exons of the uninterrupted gene are indicated in the top portion and colored to indicate the different domains of the protein that are encoded by each exon. Blue denotes the EGF-like repeats, red denotes the negative regulatory (NR) region, and green denotes the notch1 intracellular domain (ICN1). Sites at which rag mediated illegitimate recombination occur are shown as marked on the map. The regions spanned by deletions in tumors arising in Mcm2 deficient mice are also marked

where the predicted domains encoded by the resulting transcripts are indicated. In the case of tumors 7702 and 7302 in frame fusions between exons 2 and 28 are expected to result in a protein missing the majority of the EGF repeats and the NR region but containing the ICN1 domain. In the case of tumor 8002, the deletion results in a predicted truncation of the protein encoded by transcripts initiating at the normal promoter which may enhance expression from a previously identified internal promoter in exon 29 and expression of the ICN1 domain from methionine 1796 as has been observed in a prior study (Jeannet et al., 2010). Panel B shows the locations of deletions defined by sequencing amplicons containing breakpoint junctions from the Pten locus. In this case individual exons are not marked.

Notch1

5’7302

gatggggctttgggtggtagattacacactttgtaaactatgccatttg↓agccatggaaagtgcacaatgcagtgtacttaatagaggcatggattgca

3’7302

ccctaagatgtatacatataccagaaagtatggaggagtctttcttctct↓cctcattctttacccctgatttttctttgttggatattatttcaaaatca

5’ 7702

ccccagcctgcctgatacttacctgcagccagccacagtgggacaggtca↓caccccaggcaatggagtatgtggtacagaagaggcaaagtggagaagca

3’7702

gcaggcggtctctcactccttgtgccagctgccattcccagctcaggaag↓tgcttttctggaatttttttccaaggccttccctccctgtggctagtggg

5’8002

ctgccagaatggaggcacctgccgtcctacaggggacaccacccacgagt↓gtgcctgcttgccaggtaggttccatctcagtatgctggcatctagcctg

3’ 8002

tctttaccccctgatttttctttgttggatattatttcaaaatcattacta↓gagtttttttgtgtgtgttatttttttttaagagagagagagaattgatcg

Pten

5’ 7302

tgttccccctcccccacctcccagcaggtataatatctaaactgtgtcaga↓agaccgtgactacggtatgatggtgttagacgacatccgctcagcgctgc

3’ 7302

caatttctttaaaaagtagtttatttaaatgtgcaccaaagactcatttc↓tttttttccaaatatttttgtattttatatgtaagattgttctgtctgc

5’ 8102

acggatgtgagccatcatgtggatgcaagagcaagtagtctaattcactg↓aaccgtctccagctccttctgggagatttttaataccgtttcatgttcat

3’ 8102

gaagaatggcataaagttaggaaaagatgtagcattggtctgtctgtctg↓tctgtctgcctgtctgtcttctcagaatcatgaagcactaaggagtaagt

5’ 7702(+ 61 nt insertion)

atgtgatgcacaatgggattttagagagctataaaaaaataaattatcatt↓ttcaggaaaattaatgaaaactgaagatcattatggtaattaaataagca

3’ 7702

attattcaccagtagaaaatgaaacaaaaatataaaggagtgaactgagg↓aaatgctgaactatttgggctagcaaatcgaacattgactacaagaaaga

insert

aagaaattataaattataattctttaatttaatataaattatcatattttatcattttatc

Figure 4.

Sequences flanking breakpoints for deletions at the notch1 and Pten loci. 50 nt of the normal 5’ and 3’ flanking sequence relative to the deletion breakpoints (downward arrows) are shown for 3 notch1 and 3 Pten deletions where both the 5’ and 3’ breakpoints are shown for each tumor as indicated. A and T residues are colored red. The sequence of a non-templated 61 nt insertion found at the Pten breakpoint from tumor 7702 is also given.

Gene	7302	7602	7802	8002	7002	7702	7902	8102
PI3K signaling								
Pten	x	x	x	x	x	x	x	x
vav 1		a			a			a
Phldb1						x		
Inppl1							x	x
Pitpnc1							x	
Centd2					x			
Nup85					x			
Magi3								x
Nedd4		h						
Histone methylation/Set complex								
Setd1b	x	h	x	x	x	x	x	x
Wdr5/Brd3	x*	x*					x*	
Setd1a			x				x	
Ppp1r1b					x			
Mll1						x		
Histone methylation/Set independent								
dot1l	h		h			h	x	
Mllt10		a	a					
Mllt1		a			a			a
Rnf40	x		x	x		x	x	
E12/E47 Transcriptional Activation								
Tcfe2a	x	x	h	x	x	x	x	x
Notch Transcriptional Activation								
notch 1	x*			x*		x*	x*	
Gak		a			a			a
NURD Complex								
Mbd3	x	x	x	x	h	x	x	h
Gatad2a					x			
Dnmt3a						x		x
Ikzf1								x
Ikzf3		x						
Bcl11b					x	x	x	
NuRF/Histone Acetylation Complexes								
Brpf3			x	x	x	x		x
Smarcd2			x					
Myst1			x				x	
Bptf					x	x		x
Cyclin Dependent Kinase Inhibitors								
Cdkn1a			x		x			
Cdkn2a; Cdkn2b					x			x

Figure 5.

Abbreviated chart of pathways implicated by genes present in MCR deletions and amplifications and complementing non-recurrent CNVs. X, bi-allelic deletion; h, mono-allelic deletion; a, amplification; x*, short internal deletions affecting exons 5–23 in *notch1* and intron 1 in *Wdr5*. In the case of *Wdr5*, the CNV was also present in paired non-tumorous tissue and may represent heterogeneity within the strain. A complete chart including chromosomal locations, gene function and additional MCRs that do not fall into the molecular pathways indicated here is included in Supplemental Figures.

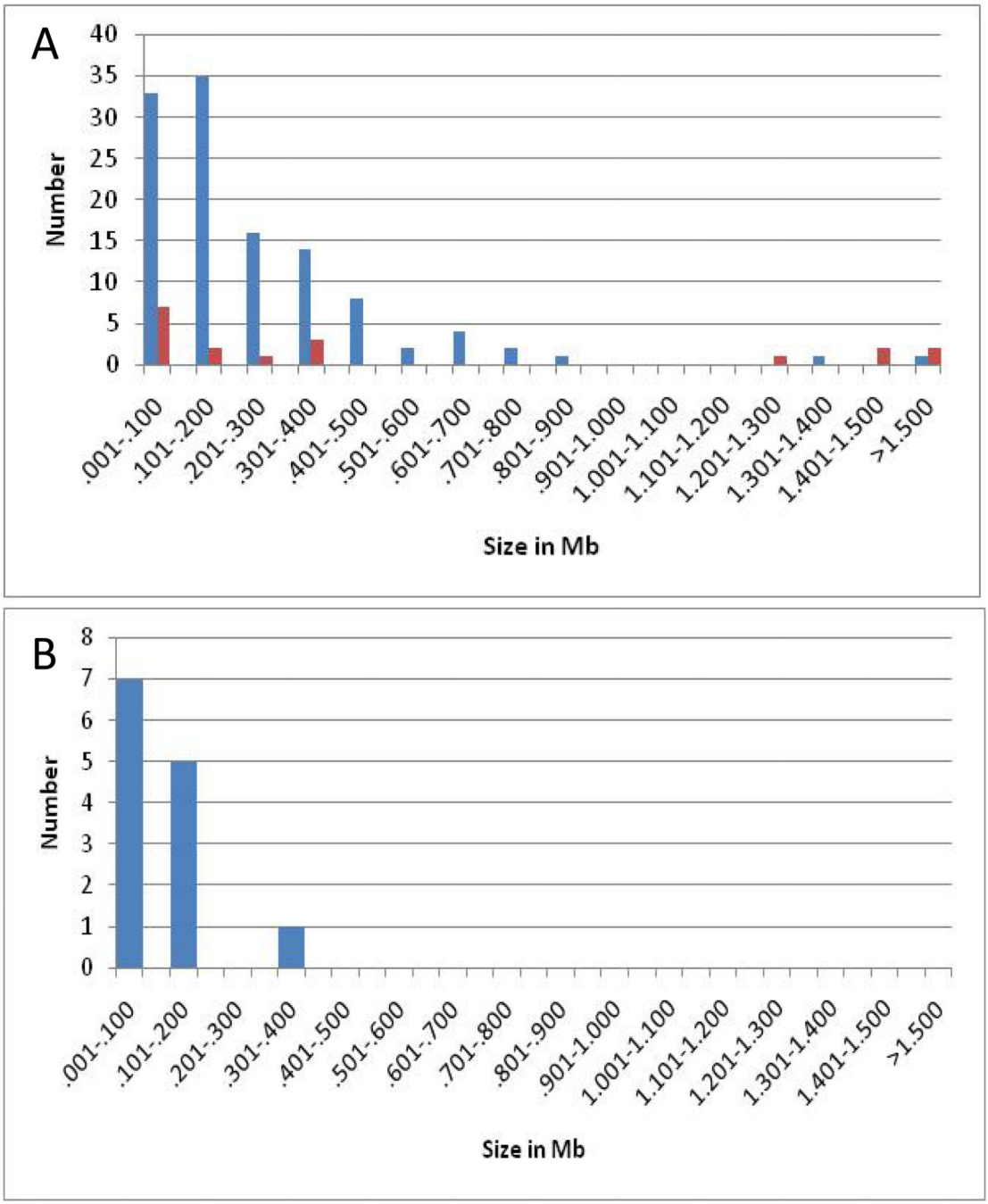

Figure 6.

Size distributions for different classes of CNVs. The frequency of CNVs of varying sizes is plotted for all deletions (blue) and amplifications (red) in panel A and for a subset of 13 non-recurrent deletions that did not contain genes related to any known oncogenic pathway and are considered to be passenger mutations in panel B.

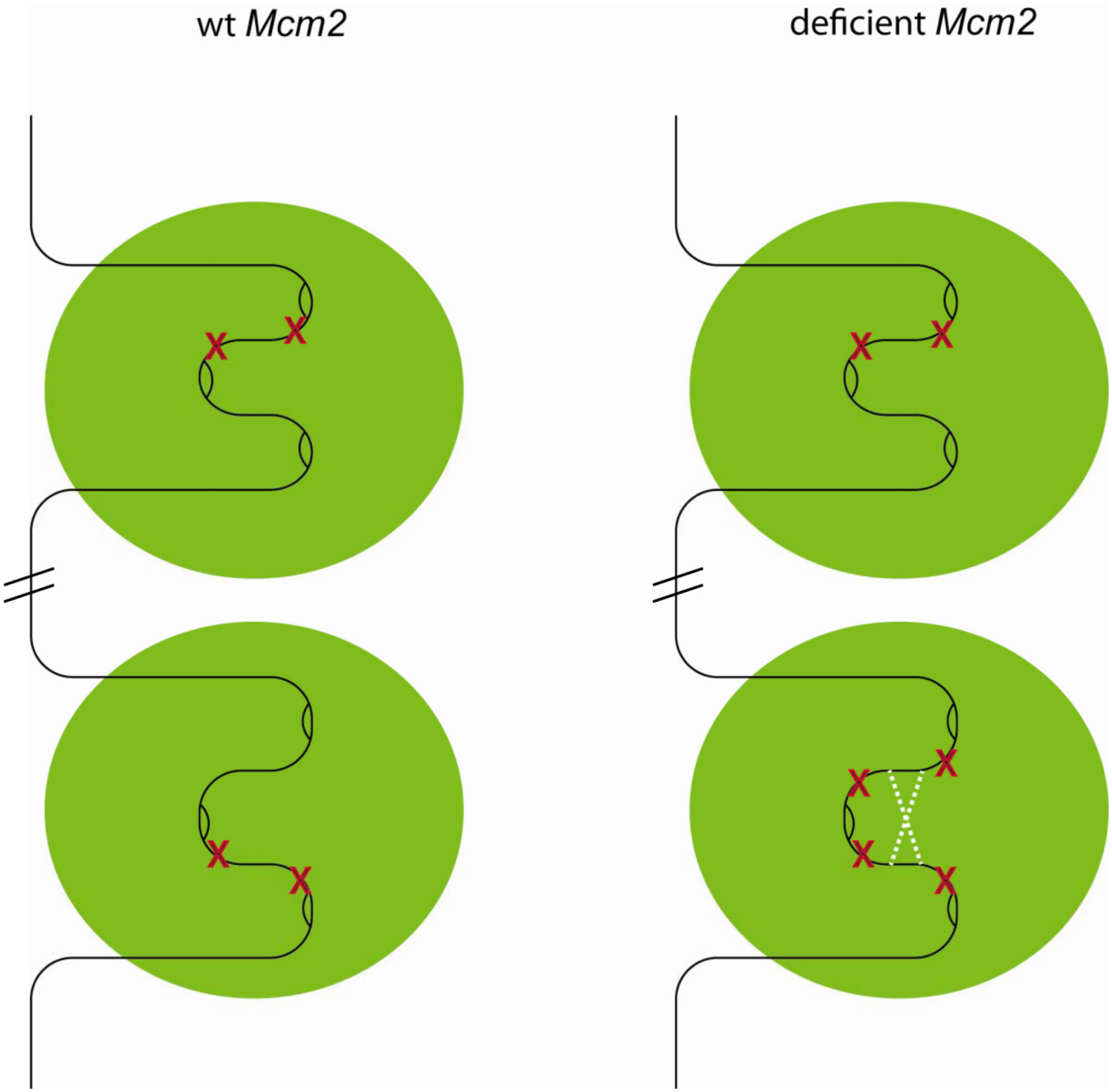

Figure 7.

Potential relationship between replicon organization and the genetic lesions produced on replication fork stalling. Replication factories are indicated by green circles, chromosomal DNA is indicated by the line running through the circles, active replicons are indicated by bubbles within the lines and sites of un-recovered stalled replication forks are indicated by the red X's. It is hypothesized that the frequency of stalled replication forks is increased by Mcm deficiency and that when the increase is sufficient that two or more stalled forks arise

within a single replication factory there is an increase in the likelihood that recombination between stalled forks will occur (indicated by dashed white lines).

Table I

Comparison of MCRs between mouse and human T-LLs

Chr	Start	End	Size	Genes in Interval	Gain/Loss	Frequency in %(haploid /diploid)	Position in Human Genome (hg17)	Ch Band	Remke et al. (2009)	Mullighan et al., (2007)	Kuiper et al., (2007)
chr4	1.33E+08	1.33E+08	0	Wasf2	Loss	25/25	chr1:27,732,126-27,816,669	1p36.11			
	1.33E+08	1.33E+08	5710	shp	Loss	37/37	chr1:27,237,976-27,240,567				
chr12	4219999	4219999	0	Cenpo	Loss	50/50	chr2:25,016,333-25,042,784	2p23.3			
	3859999	3899999	40000	Dnmt3a	Loss	25/25	chr2:25,455,846-25,564,774				
chr3*	25415559	25456523	40964	Nlgn1	Loss	50/50	chr3:173,116,244-174,001,116	3q26.31			
chr5	1.09E+08	1.09E+08	414882	Gak	Gain	37.5	chr4:843,066-926,174	4p16.3			
chr17	30287365	30181394	−105971	Zfand3	Loss	50/50	chr6:37,787,307-38,122,397	6p21.2			
	30474260	30579999	105739	Btbd9	Loss	25/25	chr6:38,136,228-38,607,924				
chr17	28829446	29219999	390553	Mapk14 Mapk13 Brpf3 Pnpla1 4930539E 08Rik Pxt1 Kctd20 Stk38 Sfrs3 AK144811	Loss	50/50	chr6:35,995,454-36,572,243	6p21.31			
chr4	88899999	89059999	160000	Cdkn2a; Cdkn2b	Loss	25/25	chr9:21,967,752-22,009,312	9p21.3	9p21.3(Loss);45/72(63%)	9p21.3(Loss); 36/50 (72%)	9p21.3(Loss); 5/7 (71%)
chr2*	27349578	27363138	13560	Wdr5	Loss	37.5/37.5	chr9:137,001,210-137,025,093	9q34.2			
chr2	26324605	26337808	13203	notch 1	Loss	50/0	chr9:139,388,897-139,440,238	9q34.3			
chr2	17972355	17988715	16360	Mllt10	Gain	25	chr10:21,823,574-22,032,555	10p12.31			
chr19	32819999	32859999	40000	Pten	Loss	100/100	chr10:89,623,195-89,728,531	10q23.31	10q23.2-23.31;4(Loss)/72(6%)	10q23.31(Loss); 3/50 (6%)	
chr7	1.09E+08	1.09E+08	−80001	Pde2a	Loss	37.5/37.5	chr11:72,287,186-72,385,494	11q13.4			
chr5	1.24E+08	1.24E+08	15244	Setd1b	Loss	100/87.5	chr12:122,242,630-122,270,561	12q24.31			
chr12	1.09E+08	1.09E+08	40000	Bcl11b	Loss	37.5/37.5	chr14:99,635,627-99,737,822	14q32.2			
chr9	72339999	72419999	80000	Rfxdc2	Loss	37.5/37.5	chr15:56,379,479-56,394,449	15q21.3			

Oncogene. Author manuscript; available in PMC 2013 March 06.

Chr	Start	End	Size	Genes in Interval	Gain/Loss	Frequency in %(haploid /diploid)	Position in Human Genome (hg17)	Ch Band	Remke et al. (2009)	Mullighan et al., (2007)	Kuiper et al., (2007)
chr7	1.35E+08	1.35E+08	116874	Phkg2 Gm166 Rnf40	Loss	62.5/62.5	chr16:30,759,737-30,786,536	16p11.2			
chr11	75019999	75099999	80000	Rtn4rl1	Loss	37.5/37.5	chr17:1,837,973-1,928,178	17p13.3		17p13.3-11.2(Loss); 2/50 (4%)	
chr11	97779999	97859999	80000	Plxdc1	Loss	25/25	chr17:37,219,556-37,307,902	17q12			
chr11	98179999	98259999	80000	Neurod2 Ppp1r1b Stard3 titin-cap Pnmt Perld1	Loss	25/25	chr17:37,760,022-37,37,844,310	17q12			
chr11	1.07E+08	1.07E+08	39999	Pecam1	Loss	25/25	chr17:62,399,864-62,401,205	17q23.3-q24.2	17q23.3(Gain);4/73 (5%)		
	1.07E+08	1.07E+08	159999	Smurf2 Kpna2 Bptf	Loss	25/25	chr17:62,540,735-65,900,956				
chr11	1.17E+08	1.17E+08	276592	Septin-9	**Loss**	25/25	chr17:75,277,492-75,496,676	17q25.2-q25.3			
chr10	79899999	79939999	40000	Tcfe2a	Loss	87.5/100	chr19:1,609,293-1,650,286	19p13.3 and 19p13.2	19p13.3(Gain);7/73 (10%) 19p13.2(Gain);4/73 (5%)		
				Mbd3	Loss	100/75	chr19:1,527,678-1,543,652				
chr17	55952968	57447177	1494209	Mllt1 Chaf1a Uhrf1 Dennd1c vav 1	Gain	37.5	chr19:6,210,393-6,,857,371				
chr2	1.53E+08	1.53E+08	9248	Asxl1	Gain	37.5	chr20:30,946,153-31,027,121	20q11.21			
chrX	1.66E+08	1.66E+08	60271	Mid1	Gain	37.5	chrX:10,413,597-10,851,809	Xp22.2			

* Also present in a subset of non-tumorous control tissues.